Reconfigurable Intelligent Surface Enabled Spatial Modulation for Visible Light Communications

Pengfei Shen and Lu Lu, *Member, IEEE*

***Abstract*—An important issue in visible light communications (VLC) is how to boost up the system throughput even when the line-of-sight (LOS) link is blocked by obstacles. In this paper, we propose reconfigurable intelligent surface (RIS) based spatial modulation (SM) designs for VLC, which enable RIS to modulate its own message on the reflected signals. Compared with conventional RIS-assisted VLC systems, RIS enabled SM VLC can further increase the overall system throughput. To enable RIS based SM for VLC, we first study two straight-forward methods by exploiting the reconfigurability of RIS whose elements are divided into groups, namely RIS enabled SM (RIS-SM) and RIS enabled generalized SM (RIS-GSM), which activate one and multiple groups, respectively. Furthermore, we find that the bit error rates (BER) performance of RIS-SM and RIS-GSM are highly affected by channel correlation. That is, there is a trade-off between the channel correlation coefficients and received signal power. To solve this problem in RIS-SM and RIS-GSM where only part of the RIS elements are active, we further propose RIS enabled receive SM (RIS-RSM), where all the RIS elements can be exploited to reflect signals. In the three proposed designs, the reflected light signals received at the destination contain two types of information streams: one is spatially modulated at the RIS node and the other is from the light source, and the two signal streams are decoded by the receiver in a joint manner using maximum-likelihood detections (MLD). We then derive the corresponding upper bounds according to BER metric for the three schemes, and simulation results verify the tightness of our analytical upper bounds. Interestingly, we find that blockage on the RIS link may have different effects for RIS-SM, RIS-GSM and RIS-RSM. Without blockage, it is shown that RIS-RSM always outperforms RIS-SM and RIS-GSM, and the SNR gain can be 30 dB when BER = 1e-6, showing the advantage of RIS-RSM for future VLC applications.**

***Index Terms*—Visible light communications, reconfigurable intelligent surface, spatial modulation, generalized spatial modulation, receive spatial modulation.**

I. Introduction

AS AN important component of 6th-Generation (6 G) technique, visible light communication (VLC), which often uses illumination devices such as light emitting diodes (LEDs) as transmitters [1], has gained significant interest recently [2], [3]. Compared with radio frequency (RF) communications, VLC can provide more spectrum resources, higher bandwidth and the potential for higher communication data rate [4]. Besides, the use of VLC will not interfere with the existing RF systems, thus it can be a good complementary technique to RF system especially for indoor scenarios.

Despite its great potential and broad prospects, VLC still has many challenges for practical applications. On the one hand, due to light's line-of-sight (LOS) communication nature, when the LOS link is blocked by obstacles, the communication capability of VLC will be much degraded. To full this gap, the use of non-LOS (NLOS) paths assisted by reconfigurable intelligent surfaces (RIS) has been taken into consideration. RIS is a class of tunable surfaces that are composed of massive artificial elements. These elements can be programmed to change the propagation environment, then the property of incident signals such as amplitude and phase can be manually controlled without consuming an additional extent of power [5]. Up to now, the concept of RIS has been widely investigated by researchers to improve the performance of the whole communication system from RF [6], [7], [8] to VLC [9], [10], [11]. In VLC systems, the NLOS propagation medium can be designed intentionally to adjust the properties of incident light – usually the reflecting direction and amplitude [12], [13] – with the aid of RIS, thus obtaining an optimized target performance, such as data rate [14], signal intensity [15], bit error rate (BER) [16] and so on.

One the other hand, the bandwidth of VLC is often limited by LED [17], and thus multiple-input–multiple-output (MIMO) techniques are often considered. Actually in practice, multiple LEDs are often equipped in VLC systems [18], [19] to provide sufficient illumination as a basic function, which exactly enables MIMO architectures. In RF communication systems, MIMO techniques are developed to increase the spectral efficiency [20], [21]. However, the spatial diversity gain is limited in indoor VLC systems, because there are no fading effects caused by atmospheric turbulence and the channel coefficient does not contain frequency and phase components [22]. Therefore, the wireless links in VLC MIMO systems can be highly correlated [22], [23]. As an analysis of this problem, in [24], the performance of different MIMO schemes for VLC is compared, including repetition coding (RC), spatial multiplexing (SMP) and spatial modulation (SM). It was shown that SM can achieve improved spectral efficiencies and is more robust to high channel correlation. Spatial modulation (SM), as a member of index modulation [25], is a combination of conventional MIMO and

Manuscript received 9 June 2023; revised 25 July 2023; accepted 2 August 2023. Date of publication 7 August 2023; date of current version 18 August 2023. This work was supported in part by the Key Research Program of the Chinese Academy of Sciences under Grant ZDRW-KT-2019-1-0103. *(Corresponding author: Lu Lu.)*

The authors are with the Key Laboratory of Space Utilization, Technology and Engineering Center for Space Utilization, Chinese Academy of Sciences, Beijing 100094, China, and also with the University of Chinese Academy of Sciences, Beijing 100190, China (e-mail: shenpengfei19@mails.ucas.ac.cn; lulu@csu.ac.cn).

Digital Object Identifier 10.1109/JPHOT.2023.3302409

digital modulation techniques [26], [27]. For a transmitter with multiple antennas, SM only activates one of them and the index of the active antenna can be used to convey information, thus a new modulation dimension – spatial domain is added to the system and the spectral efficiency can be enhanced [28]. Based on the principle of SM, a number of variants have been developed, such as generalized SM (GSM), receive SM (RSM) and so on [29].

To combine the best of RIS and SM techniques in VLC systems, we propose RIS based SM schemes in this paper to boost up the data transmission rates of VLC even when its LOS link is blocked by obstacles.

A. Related Works

The techniques of using SM in VLC systems have been widely investigated in the existing literature. In [30], the authors proposed an optical spatial modulation (OSM) scheme, where only one transmitter is active to send data. In [31], the GSM scheme is proposed for VLC, where multiple transmitters can be active, each sending different data. Compared with SM, GSM provides a higher spectral efficiency. In [32], the BER performance of SM and GSM are evaluated by both analytical and simulation results. To further enhance spectral efficiency, an extension of GSM called improved GSM (iGSM) was proposed in [33]. Moreover, to reduce performance loss caused by the highly correlated optical MIMO channels, an LED-grouping based SM scheme was proposed to alleviate the channel correlation in VLC [34], where LEDs with strong correlation properties are classified into the same group. In [35], the authors optimized the constellation symbols to realize the maximization of average mutual information in GSM based VLC system. And in order to further improve the system BER performance, the authors in [36] proposed an SM scheme with space time block codes (STBC) and analyzed its performance of BER and achievable rate. In the above works, spatial modulation techniques are executed at the transmitter side, which are lack of flexibility, and the data rate is restricted by the number of transmitters.

As RIS can manipulate the signals propagating in the wireless channel, it can be also used to implement SM in the reflecting path to send its own data. Compared with the conventional SM schemes, RIS enabled SM does not need power amplifiers to generate new signals, making it more flexible and suitable for scenarios where the transmitted power is limited or massive devices need to send data. This concept has been developed and analyzed in RF communications, where RIS can be used to simultaneously perform passive beamforming and information transfer (PBIT) [29], [37], [38], [39], [40], [41], [42], [43], [44], [45], in which the information transfer is often realized by designing the ON and OFF states of the reflecting elements. In [37], the concept of RIS based SM is proposed and its performance is analyzed. In [38], the authors proposed PBIT by adopting SM on RIS elements. In [39], a reflection pattern modulation scheme is proposed, where different reflection patterns of RIS are employed for PBIT. In [40], the authors developed a scheme to perform SM at both transmitter and receiver for a higher spectral efficiency, and a closed-form of average BER bound is derived. Other kinds of spatial modulation schemes for RIS based communication system have also been proposed, such as differential reflecting modulation [41], generalized spatial modulation [42], and quadrature reflection modulation [43].

Similarly, RIS enabled SM schemes can also be applied to VLC. This concept has been proposed in [9] based on the principle as in RF communications. However, only SM is introduced and there is no further analysis of this system. A comparison of the listed works and our work is summarized in Table I.

TABLE I
CATEGORY OF THE RELATED WORKS

Communication systems		RIS enabled RF	VLC	
			without RIS	with RIS
Non-SM systems		[6]–[8]	[1], [4]	[9]–[16]
SM systems	SM	[29], [37], [38], [40]	[24], [30], [36]	[9], this work
	GSM	[29], [39], [42]	[31]–[35]	this work
	RSM	[29], [40]	[46]	

B. Contributions

In this paper, we propose and analyze RIS based spatial modulation schemes in VLC. Specifically, we propose RIS enabled spatial modulation (RIS-SM[1]) and RIS enabled generalized spatial modulation (RIS-GSM). Each symbol from LED can be chosen from a positive real number set, and sent to RIS in the NLOS path. For RIS node, its elements are equally divided intoN_g groups and only part of them are activated to carry on spatial modulation, where the index of the chosen group contains the data from RIS. After that, the light is reflected to the receiver, where maximum likelihood detection (MLD) is executed to get data from both LED and RIS. The designs expand the scope of applications of RIS by making it a data transmitter. Compared with conventional spatial modulation techniques in VLC, RIS enabled spatial modulation schemes are easier to realize higher data rates by adjusting N_g.

In RIS-SM and RIS-GSM, not all the RIS groups are employed to reflect signals in order to perform different patterns for spatial modulation. Besides, the channel correlation can be high in VLC as stated before. These issues will lead to a severe degradation of the system BER performance. To full this gap, we put forth RIS enabled receive spatial modulation (RIS-RSM), where all RIS groups are turned on, but they reflect the incident light to only one of the receivers, whose index represents the data from RIS. In RIS-RSM, there is no channel correlation problem and the reflected signals can be fully employed, making it outperform the other two schemes. Furthermore, based on the union bound methods, we derive the closed form expressions of upper bounds on the BER of the proposed three RIS enabled spatial modulation schemes, and we validate our analysis by simulation results.

The main contributions of this paper are listed as follows:

1) To increase the system throughput of VLC even when its LOS link is blocked, we propose three RIS based spatial modulation schemes as combinations of RIS and spatial

[1]To avoid confusion, in the following the term "SM" refers to the systems in which only one of the transmitters (or RIS groups) are turned on, while "spatial modulation" has a broader meaning that contains SM, GSM, RSM and so on.

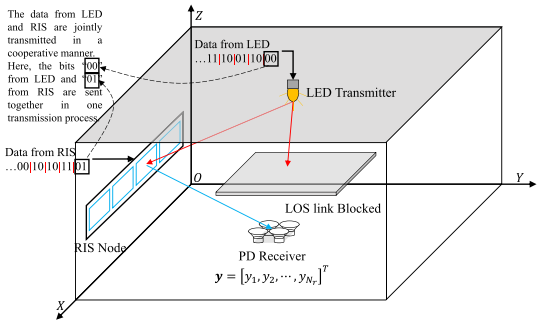

Fig. 1. System model of RIS enabled spatial modulation scheme.

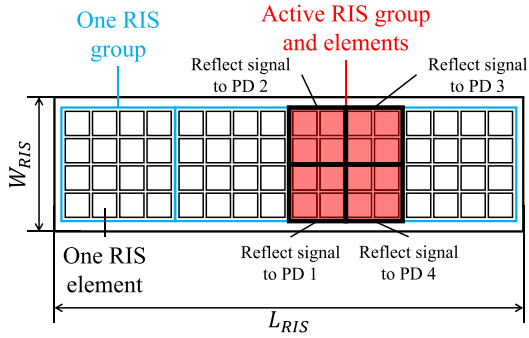

Fig. 2. Illustration of RIS elements and groups.

modulation techniques. Specifically, we propose RIS-SM, RIS-GSM, and RIS-RSM, where the former two only activate part of the RIS groups to represent data, while in RIS-RSM, all the RIS groups can reflect the light to only one of the receivers.

2) We derive the closed form expressions of the BER for the proposed RIS enabled spatial modulation schemes based on the union bound methods, and Monte Carlo simulations are carried out in order to validate our derived analytical results.
3) Based on the simulation results, we analyze the influence of channel correlation and show that it has a large impact on the the dominating source of errors, and there is a trade-off between channel correlation coefficients and receive signal power when adjusting the size of RIS for RIS-SM. Furthermore, we find that RIS-RSM can make full use of the RIS reflecting signals, and it outperforms the other two schemes for all setting-ups.
4) We evaluate the system BER with different levels of blockage on the NLOS links (namely, the links between RIS and PDs). For RIS-SM where only one RIS group is active in each transmission, link blockage can help improve the BER performance, since the channel correlation is reduced among different groups by blockage. While for RIS-RSM where the channel correlation is not important, link blockage may, on the other hand, cause BER degradation because of the loss of power on the PD receiver.

II. System Model

We consider a VLC system consisting of an LED transmitter, a RIS node and a PD receiver which are placed in a room, as shown in Fig. 1. The transmitter uses one LED to send the visible light signal which contains the data from itself, and the receiver uses a PD array consisting of N_r PDs to receive the light signal. We assume that the LOS link between the LED and PD is blocked, thus the NLOS link through the RIS node is employed for communication. By manipulating the RIS elements individually to change the reflected directions of the incident light, the NLOS link, i.e., LED-RIS-PD, is active for communication.

At the RIS node, spatial modulation is used, which means that RIS can also send its own data to the PD array utilizing the light from LED. The number of RIS elements is denoted by N_e, and they are equally divided into N_g groups. Each group has N_e/N_g elements which are placed aligned in a quadratically $\sqrt{N_e/N_g} \times \sqrt{N_e/N_g}$ array. Here we assume N_e/N_g and $\sqrt{N_e/N_g}$ are both integers, and denote the length and width of RIS node by L_{RIS} and W_{RIS}, respectively, as shown in Fig. 2. In our system, RIS is assumed to be a passive device, i.e., it only adjusts the reflecting direction of incident light without changing its amplitude [16].

As shown in Fig. 1, the system comprises two data streams: one from LED and the other from RIS. We assume that LED employs M-level pulse amplitude modulation (M-PAM) scheme [47], allowing it to transmit $\log_2(M)$ bits in each transmission process. On the other hand, the RIS node utilizes spatial modulation techniques to modulate its own data onto the reflected signals. Take RIS-SM as an example, in each transmission, one of the RIS groups is selected and its index is employed to represent the data to be transmitted by RIS. In the chosen group, all elements can reflect the light to PD, while those in other groups are turned off and cannot reflect the light. For simplicity, we call the RIS groups which reflect signals to PD array as "active" groups, and the elements in these groups are "active" elements. At the RIS node, each active element in the active group can be used to reflect the incident light signal, and the reflecting direction can be manually adjusted, such that the light reflected by each element can only reach at most one of the PDs [48]. As one RIS group can have many elements, it then has the ability to contact with all the N_r PDs by setting different elements in the group to reflect light to different PDs. Here we assume that N_e/N_g is also a multiple of N_r, then each PD can receive signals reflected by $N_e/(N_g N_r)$ elements in the active group. We provide an example in Fig. 2 to show how one RIS group reflects light to all the PDs, where there are 16 elements in each RIS group and 4 PDs to receive the light signal. In each transmission, every 4 elements in the active group reflect the incident light from LED to one of the PDs, then all the 16 elements can send the light to all the 4 PDs simultaneously.

The reflected signals contain two kinds of data: from LED and from RIS. At the receiver side, both the data from LED and RIS are jointly detected based on the received signals by PD array, which can be represented by

$$\mathbf{y} = r\mathbf{H}\mathbf{s}_{\text{RIS}} \cdot s_{\text{LED}} + \mathbf{n} = r\mathbf{H}_{\text{RIS}} \cdot s_{\text{LED}} + \mathbf{n}, \quad (1)$$

where $\mathbf{n}$ is real valued additive white Gaussian noise (AWGN) with zero mean and a variance σ^2; r is the optical-to-electrical conversion coefficient; $\mathbf{s}_{\text{RIS}}$ contains the data from RIS and will be elaborated in Section III; $\mathbf{H}_{\text{RIS}} \triangleq \mathbf{H}\mathbf{s}_{\text{RIS}}$ is used to represent the signal in the spatial domain; s_{LED} is an M-PAM signal generated by LED and it is chosen from a set of intensity levels given by

$$S_{\text{LED}} = \left\{ \frac{2I}{M+1} m, m = 1, 2, \ldots, M \right\}, \tag{2}$$

where I is the mean optical power emitted. The channel matrix $\mathbf{H}$ is given by

$$\mathbf{H} = \begin{bmatrix} h_{11} & \cdots & h_{1N_g} \\ \vdots & \ddots & \vdots \\ h_{N_r 1} & \cdots & h_{N_r N_g} \end{bmatrix}, \tag{3}$$

where h_{ig} $(i = 1, 2, \ldots, N_r,\ g = 1, 2, \ldots, N_g)$ represents the NLOS channel gain between LED and the i-th PD through the g-th RIS group, which can be calculated as $h_{ig} = \sum_{j=1}^{N_e/N_g} h_{ig,j}$, where $h_{ig,j}$ is the NLOS channel gain through the j-th RIS element in the g-th group and it can be calculated by [49]

$$h_{ig,j} = \begin{cases} \frac{(k+1)A}{2\pi(d_{L,gj}+d_{gj,i})^2} \cos^k(\phi_{g,j}) \cos(\psi_i), \\ \qquad \text{if } 0 \le \psi_i \le FOV \text{ and } \mathcal{I}(j,i) = 1; \\ 0, \qquad \text{otherwise}, \end{cases} \tag{4}$$

where $\mathcal{I}(j,i)$ indicates whether the j-th element can reflect signal to the i-th PD: $\mathcal{I}(j,i) = 1$ means there is a connection, and $\mathcal{I}(j,i) = 0$ means not. FOV is the field of view of each PD; A is the detector area; $\phi_{g,j}$ is the emergence angle of LED; ψ_i is the incidence angle of the i-th PD; $d_{L,gj}$ is the distance between LED and the j-th RIS element; $d_{gj,i}$ is the distance between the i-th PD and the j-th RIS element in the g-th group; and $k = -\frac{\ln 2}{\ln(\cos(\Phi_{1/2}))}$, where $\Phi_{1/2}$ is the transmitter semi-angle.

III. RIS Enabled Spatial Modulation Techniques

In this section, we introduce three RIS enabled spatial modulation schemes, i.e., RIS enabled spatial modulation (RIS-SM), RIS enabled generalized spatial modulation (RIS-GSM), and RIS enabled receive spatial modulation (RIS-RSM). For RIS-SM and RIS-GSM, only part of the RIS groups are active to reflect the incident signal to all the PDs, and the indexes of active groups are used to represent data from RIS. For RIS-RSM, all RIS groups are active but they reflect the light to only one of the PDs whose index represents the data. With respect to Fig. 1, where both LED and the RIS node can transmit two bits at a time. In the first transmission, LED sends data '00' and RIS sends data '01'. If RIS-SM is employed, the second RIS group is activated, allowing it to reflect signals from LED to all the PDs; while for RIS-RSM, all RIS groups can reflect signals, but only PD2 receives the signals. Then at the PD receiver, the data '00' and '01' will be jointly decoded using MLD and the first transmission is finished. Note that although only part of the RIS groups (or PDs) are utilized in each transmission, for consecutive packet transmission, all RIS groups and PDs will be used.

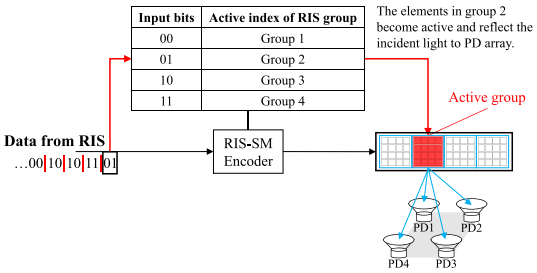

Fig. 3. Operation of RIS-SM with $N_g = 4$ and $N_r = 4$.

A. RIS-SM and RIS-GSM

For RIS-SM, only one RIS group is active to reflect the signal at each moment, and the index of the active group is determined by the data from RIS, thus the data is transmitted in the spatial domain, as shown in Fig. 3. In this scheme, the bit per channel use (bpcu) is $\log_2(M) + \log_2(N_g)$, where we assume that N_g is a power of 2. Then the signal $\mathbf{s}_{\text{RIS}}$ can be represented by a $N_g \times 1$ vector chosen from a set given by

$$\mathbf{S}_{\text{RIS-SM}} = \{\mathbf{e}_g, g = 1, 2, \ldots, N_g\}, \tag{5}$$

where $\mathbf{e}_g$ is the g-th column vector of the $N_g \times N_g$ identity matrix. Then $\mathbf{s}_{\text{RIS}}$ is a column vector with only one non-zero element which equals to 1 representing the active group of RIS and other elements in the vector are all 0. And we have

$$\mathbf{H}_{\text{RIS-SM}} \in \{\mathbf{h}_g, g = 1, 2, \ldots, N_g\},$$

where $\mathbf{H}_{\text{RIS-SM}} = \mathbf{H}\mathbf{s}_{\text{RIS}}$ is defined in (1) and $\mathbf{h}_g$ is the g-th column of channel matrix $\mathbf{H}$ in (3). An example of RIS-SM is shown in Fig. 3, in which $N_g = 4$ and $N_r = 4$.

In each transmission, given the RIS data to be sent, the channel gain is $\mathbf{h}_g$, whose i-th element represents the channel gain of i-th PD $(i = 1, 2, \ldots, N_r)$. Then the average channel gain through all the PDs can be expressed as

$$G_{\text{RIS-SM}} = \frac{1}{N_g N_r} \sum_{g=1}^{N_g} \sum_{i=1}^{N_r} h_{ig}, \tag{6}$$

where h_{ig} is defined in (3).

Remark: The channel correlation can be evaluated by the normalized instantaneous channel correlation matrix (NICCM) $\mathcal{M}$ [34], whose element $[\mathcal{M}]_{ij}$ is calculated by

$$[\mathcal{M}]_{ij} = \frac{\mathbf{h}_i^T \mathbf{h}_j}{\|\mathbf{h}_i\|_2 \cdot \|\mathbf{h}_j\|_2},$$

where $\mathbf{h}_i$ is the i-th column vector of channel matrix $\mathbf{H}$ in (3) and $\|\cdot\|_2$ represents the Euclidean norm. The value of $[\mathcal{M}]_{ij}$ denotes the correlation property of channels through the i-th and j-th RIS group – a large value means they are highly correlated.

The major drawback of RIS-SM is that only one RIS group can be active at each moment, thus resulting in a high path loss at RIS side. Besides, the channel coefficient vectors of different RIS groups can be similar, causing a high correlation. This is also a severe issue affecting the performance. To fill this gap,

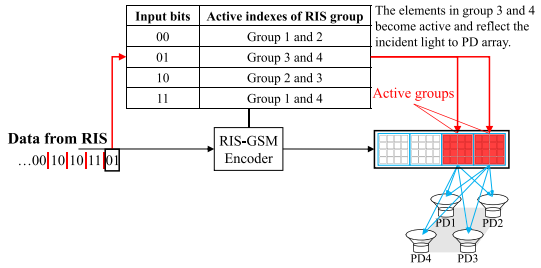

Fig. 4. Operation of RIS-GSM with $N_g = 4$, $N_a = 2$, and $N_r = 4$.

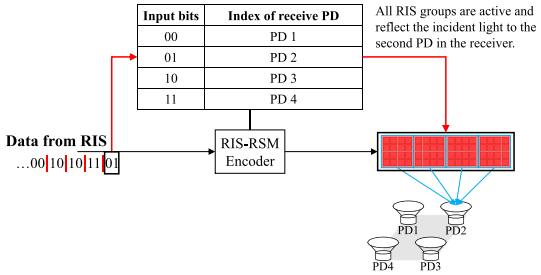

Fig. 5. Operation of RIS-RSM with $N_g = 4$ and $N_r = 4$.

we propose RIS-GSM, where more than one RIS groups can be active, as shown in Fig. 4. Denote by N_a the number of active groups and $1 \leq N_a < N_g$, then there are total $\binom{N_g}{N_a}$ patterns that can be chosen for representing data. However, as $\binom{N_g}{N_a}$ may not be a power of 2, some of the patterns can be neglected. For example, when $N_g = 4$ and $N_a = 2$, there are total $\binom{4}{2} = 6$ possible active patterns, while only 4 patterns are needed. A selection of active patterns is shown in Fig. 4.

Different from the conventional GSM scheme in VLC, the data in the signal domain transmitted by different active groups are the same, because all the RIS groups reflect the same incident light generated by LED. Then the bpcu of RIS-GSM is $\log_2(M) + \lfloor \log_2 \binom{N_g}{N_a} \rfloor$, where $\lfloor x \rfloor$ is the floor function which returns the nearest integer no more than x. To simplify the expression, we define $N_g' \triangleq 2^{\lfloor \log_2 \binom{N_g}{N_a} \rfloor}$, then the bpcu is $\log_2(M) + \log_2(N_g')$.

The transmitted signal $\mathbf{s}_{\text{RIS}}$ in RIS-GSM can also be represented by a $N_g \times 1$ vector whose elements equal to 1 or 0, and 1 means the corresponding RIS group is active. All the possible vectors $\mathbf{s}_{\text{RIS}}$ form a set $\mathbf{S}_{\text{RIS-GSM}}$ with total $\log_2(N_g')$ elements. Take Fig. 4 as an example, the set $\mathbf{S}_{\text{RIS-GSM}}$ can be written as

$$\mathbf{S}_{\text{RIS-GSM}} = \left\{ [1,1,0,0]^T, [0,0,1,1]^T, [0,1,1,0]^T, [1,0,0,1]^T \right\}, \tag{7}$$

and we have

$$\mathbf{H}_{\text{RIS-GSM}} \in \{\mathbf{h}_1 + \mathbf{h}_2, \mathbf{h}_3 + \mathbf{h}_4, \mathbf{h}_2 + \mathbf{h}_3, \mathbf{h}_1 + \mathbf{h}_4\}.$$

Compared with RIS-SM, RIS-GSM has the ability to send data at a higher data rate without changing the grouping method of RIS, thus achieving an enhanced spectral efficiency, and RIS-SM can be viewed as a special case of RIS-GSM for $N_a = 1$. Besides, RIS-GSM can help reduce the impact of channel correlation in RIS-SM by setting the patterns combining the channels with similar coefficients. Similarly, we can also get the average channel gain of RIS-GSM as

$$G_{\text{RIS-GSM}} = \frac{N_a}{N_g N_r} \sum_{g=1}^{N_g} \sum_{i=1}^{N_r} h_{ig}. \tag{8}$$

As can be seen, the power gain of RIS-GSM is higher than that of RIS-SM because of the more active RIS groups.

We remark that the channel correlation can be evaluated by the normalized instantaneous channel correlation matrix (NICCM) $\mathcal{M}$ [34], whose element $[\mathcal{M}]_{ij}$ is calculated by $[\mathcal{M}]_{ij} = (\mathbf{H}_i^T \mathbf{H}_j)/(\|\mathbf{H}_i\|_2 \cdot \|\mathbf{H}_j\|_2)$, where $\mathbf{H}_i$ is the i-th column vector of channel matrix $\mathbf{H}$ in (3) and $\|\cdot\|_2$ represents the Euclidean norm. The value of $[\mathcal{M}]_{ij}$ denotes the correlation property of channels through the i-th and j-th RIS group – a large value means they are highly correlated.

B. Ris-Rsm

In RIS-SM and RIS-GSM, there exists a power loss at the RIS node because not all groups are active to present different reflecting patterns. Besides, the similarity between the channel gains through different RIS groups bring the channel correlation problem. To address these issues, we propose RIS-RSM, where all the RIS groups are active to reflect the light. In this way, an enhanced receive power can be obtained and the receiver do not need to distinguish which RIS group is active for reflection. However, the spatial information of active RIS groups then cannot carry data bits from the RIS node. To perform spatial modulation, we utilize the different space information of receivers, i.e., all the RIS elements can be controlled to reflect the light to only one of the PDs. In each transmission, there will be only one of the PDs that can get the reflected signals from RIS, while other PDs cannot. By detecting the index of which PD receives the light signals while others do not, the corresponding $\log_2(N_r)$ data bits from RIS can be obtained, as shown in Fig. 5. Although all the PDs are employed to receive successive packets, in each transmission process only one is used. Hence, there is no correlation for the receiver in RIS-RSM. The bpcu of RIS-RSM is $\log_2(M) + \log_2(N_r)$, where we assume N_r is a power of 2.

In RIS-RSM, all the RIS groups are active, thus the PD array receives the signals reflected from all elements, and we have

$$\mathbf{H}_{\text{RIS-RSM}} \in \{\mathbf{h}_{\text{sum},i}, i = 1, 2, \ldots, N_r\}, \tag{9}$$

where $\mathbf{h}_{\text{sum},i}$ is the i-th column vector of a $N_r \times N_r$ diagonal matrix whose diagonal elements are

$$\sum_{g=1}^{Ng} h_{1\,g}, \sum_{g=1}^{Ng} h_{2\,g}, \ldots, \sum_{g=1}^{Ng} h_{N_r g}.$$

An example of RIS-RSM is shown in Fig. 5, in which $N_g = 4$ and $N_r = 4$.

The average power gain of RIS-RSM is given by

$$G_{\text{RIS-RSM}} = \frac{1}{N_r}\sum_{g=1}^{N_g}\sum_{i=1}^{N_r} h_{ig}. \tag{10}$$

According to (6), (8) and (10), we have $G_{\text{RIS-GSM}} = N_a G_{\text{RIS-SM}}$ and $G_{\text{RIS-RSM}} = N_g G_{\text{RIS-SM}}$, and we remark that RIS-SM has the smallest value among three schemes, since only one RIS group is active. For RIS-GSM and RIS-RSM, the numbers of active groups are N_a and N_g, respectively, leading to larger power gain values.

Compared with RIS-SM and RIS-GSM, RIS-RSM can take full advantage of RIS elements, thus it has the maximum receive energy among the three schemes. Besides, RIS-RSM will not suffer from degradation caused by channel correlation, which can make it perform better. However, the data rate of RIS-RSM is limited by the number of PDs, thus can not be set flexibly as the other two schemes, which is a drawback of RIS-RSM.

C. Performance Analysis

At the receiver, the MLD is used to get the data from both LED and the RIS node that has the minimum Euclidean distance between the received signal, which is given by

$$\hat{\mathbf{s}} = \arg\min_{\mathbf{s}\in\mathbf{S}} \|\mathbf{y} - r\mathbf{H}_{\text{RIS}}\cdot s_{\text{LED}}\|_2^2, \tag{11}$$

where $\mathbf{s} \triangleq \mathbf{H}_{\text{RIS}}\cdot s_{\text{LED}}$ is the signal containing the data from both LED and RIS; $\mathbf{S}$ is the set consists of all the possible signals $\mathbf{s}$; $s_{\text{LED}} \in S_{\text{LED}}$ and S_{LED} is defined in (2). In RIS-SM and RIS-GSM, $\mathbf{H}_{\text{RIS}} = \mathbf{H}\mathbf{s}_{\text{RIS}}$, $\mathbf{s}_{\text{RIS}} \in \mathbf{S}_{\text{RIS-SM}}$ for RIS-SM and $\mathbf{s}_{\text{RIS}} \in \mathbf{S}_{\text{RIS-GSM}}$ for RIS-GSM. While for for RIS-RSM, $\mathbf{H}_{\text{RIS}}$ is chosen form the set defined in (9).

The cardinalities of set $\mathbf{S}$, denoted by $|\mathbf{S}|$, for the three schemes are given by

$$|\mathbf{S}| = 2^{\text{bpcu}} = \begin{cases} N_g M, & \text{for RIS-SM},\\ N_g' M, & \text{for RIS-GSM},\\ N_r M, & \text{for RIS-RSM}, \end{cases}$$

1) Complexity Analysis: MLD is an optimal detector for spatial modulation systems and has been widely studied [50], [51]. We first analyze the computational complexity of MLD in (11) for our proposed schemes. Note that in VLC, the received signals at the PD array are all real numbers, then for each $\mathbf{s}\in\mathbf{S}$, calculating $\|\mathbf{y} - r\mathbf{H}_{\text{RIS}}\cdot s_{\text{LED}}\|_2^2$ requires N_r multiplications (here we assume that each value of $r\mathbf{H}_{\text{RIS}}\cdot s_{\text{LED}}$ has been known in advance and does not need to be calculated again in the decoding process). Then the computational complexity of MLD is given by

$$\mathcal{C}_{\text{MLD}} = N_r\,|\mathbf{S}| = \begin{cases} N_r N_g M, & \text{for RIS-SM},\\ N_r N_g' M, & \text{for RIS-GSM},\\ N_r^2\, M, & \text{for RIS-RSM}. \end{cases} \tag{12}$$

2) BER Analysis: Now we derive the upper bounds on the BER of MLD in (11) for the proposed RIS enabled spatial modulation designs for VLC. First of all, we calculate the pairwise error probability (PEP), which is defined as the probability that the receiver mistakes the transmitted data $\mathbf{s_1}$ for another data $\mathbf{s_2}$ given knowledge of the channel matrix $\mathbf{H}$, and it is given by

$$\begin{aligned}\text{PEP} = \Pr(\mathbf{s_1}\to\mathbf{s_2}|\mathbf{H}) = &\quad \|\mathbf{y}-\mathbf{p_1}\|_2^2 > \|\mathbf{y}-\mathbf{p_2}\|_2^2\\ = Q&\left(\sqrt{\frac{\|\mathbf{p_1}-p_2\|_2^2}{4\sigma^2}}\right),\end{aligned} \tag{13}$$

where $Q(x) \triangleq \frac{1}{\sqrt{2\pi}}\int_x^{+\infty} e^{-\frac{1}{2}t^2}dt$ is the Q-function; $\mathbf{p_i}$ is the corresponding receive constellation point of signal $\mathbf{s_i}$ given by

$$\mathbf{p} = \begin{cases} r\mathbf{H}\mathbf{s}_{\text{RIS}}\cdot s_{\text{LED}} \text{ and } \mathbf{s}_{\text{RIS}}\in\mathbf{S}_{\text{RIS-SM}}, & \text{for RIS-SM};\\ r\mathbf{H}\mathbf{s}_{\text{RIS}}\cdot s_{\text{LED}} \text{ and } \mathbf{s}_{\text{RIS}}\in\mathbf{S}_{\text{RIS-GSM}}, & \text{for RIS-GSM};\\ r\mathbf{H}_{\text{RIS}}\cdot s_{\text{LED}} \text{ and } \mathbf{H}_{\text{RIS}}\in\mathbf{H}_{\text{RIS-RSM}}, & \text{for RIS-RSM}. \end{cases} \tag{14}$$

Using PEP, an upper bound on the BER can be obtained by union bound methods [52], which is given by

$$\text{BER} \le \frac{1}{\text{bpcu}\cdot 2^{\text{bpcu}}}\sum_{\mathbf{s_1}}\sum_{\mathbf{s_2}} d_H(\mathbf{s_1},s_2)\cdot Q\left(\sqrt{\frac{\|\mathbf{p_1}-p_2\|_2^2}{4\sigma^2}}\right), \tag{15}$$

where $d_H(\mathbf{s_1},s_2)$ is the Hamming distance between the bits of $\mathbf{s_1}$ and $\mathbf{s_2}$.The upper bounds on the BER of RIS-SM, RIS-GSM and RIS-RSM can be written as in (16), (17) and (18), shown at the bottom of the next page, respectively, $s_{\text{LED}}(m)$ represents the m-th element of set S_{LED}, $\mathbf{s}_{\text{RIS-SM}}(g)$ in (16) and $\mathbf{s}_{\text{RIS-GSM}}(g)$ in (17) are the g-th elements of $\mathbf{S}_{\text{RIS-SM}}$ and $\mathbf{S}_{\text{RIS-GSM}}$, respectively. $\mathbf{h}_{\text{sum},i}$ in (18) is defined in (9). As can be seen, the three proposed schemes have similar expressions of upper bounds on BER, but they have different summation numbers due to their different operating principles.

D. Link Blockage

It has been demonstrated in [24] that the performance of SM can be greatly improved when link blockage is present. This improvement arises from the reduced channel correlation, which compensates for the loss of received power. Despite the decrease in received power due to blockage, the lower channel correlation can enhance the overall performance of spatial modulation.

Considering the link blockage, the NLOS channel gain between the LED and the i-th ($i = 1,2,\ldots,N_r$) PD through the j-th ($j = 1,2,\ldots,N_e/N_g$) RIS element in the g-th ($g = 1,2,\ldots,N_g$) RIS group becomes a random variable denoted by $\widetilde{h}_{ig,j}$, whose probability distribution is given by [53], [54]

$$\begin{cases} \Pr(\widetilde{h}_{ig,j} = 0) = 1-\mathcal{N},\\ \Pr(\widetilde{h}_{ig,j} = h_{ig,j}) = \mathcal{N}, \end{cases} \tag{19}$$

where $(1-\mathcal{N})$ is the probability of obstacle, $\mathcal{N} = \exp(-Td_{gj,i})$, T is obstacle probability coefficient, $h_{ig,j}$ and $d_{gj,i}$ have been defined in (4). That is, the channel gain is 0 when the channel is blocked with probability $(1-\mathcal{N})$, otherwise it equals to $h_{ig,j}$. Here we assume that only the links between RIS elements and PDs can be blocked.

TABLE II
SIMULATION SETUP

Parameter names	Symbols	Values
Number of PD	N_r	4
Number of RIS elements	N_e	256
Number of RIS groups	N_g	4
Detector area	A	1cm^2
Transmitter semi-angle	$\Phi_{1/2}$	60°
field of view of PD	FOV	85°
Optical-to-electrical conversion coefficient	r	1
M-PAM	M	4
Size of RIS	$L_{RIS} \times W_{RIS}$	2m × 0.5m
LED location	(2.5m, 2.5m, 2.5m)	
Center of RIS	(2.5m, 0m, 1.5m)	
Center of PD array	L1: (2.5m, 2.5m, 0.5m) L2: (2.5m, 0.5m, 0.5m)	

Based on the distribution of $\widetilde{h}_{ig,j}$, we can analyze the influence induced by different levels of blockage, and the corresponding simulation results are shown in Fig. 4.

IV. SIMULATION RESULTS AND ANALYSIS

In this section, we compare and analyze the performance of the proposed RIS enabled spatial modulation systems. We consider an indoor scenario located in a room with size of 5 m ×5 m×3 m. For the sake of description, a corner of room is selected as the origin of coordinates, as shown in Fig. 1. RIS is placed at the center of *XZ*-plane, its long side is parallel to the *X*-axis, and the RIS groups are divided along this side. The receiver uses 4 PDs that are aligned in a quadratically 2 × 2 array with spacing $d_{RX} = 0.1$ m. For RIS-GSM scheme, we set $N_a = 2$ and select patterns for data transmission in spatial domain as in (7). Other parameter settings are mainly referred to [24], [31] and they are presented in Table II unless specified otherwise. And we show more detailed information about parameter settings in Table III.

TABLE III
DETAILED SIMULATION PARAMETER SETTINGS USED IN DIFFERENT SYSTEMS

Parameters	Conventional RIS-assisted VLC system (benchmark)	RIS-SM	RIS-GSM	RIS-RSM
bpcu	4	4	4	4
Number of LED	1	1	1	1
M-PAM used by LED	16	4	4	4
Number of active RIS groups in each transmission	4	1*	2*	4
Number of PDs to receive reflected signals in each transmission	4	4	4	1*

∗ The numbers with this superscript mean that the corresponding active RIS groups (PDs) in each transmission process are dependent on the data to be sent by RIS.

As can be seen, modulation orders of both LED and RIS are the same for all the systems, i.e., they have the same bpcu for a fair comparison.

To strengthen our evaluation, we also add a benchmark using conventional RIS-assisted VLC links in which RIS only reflects the light signal without performing spatial modulation. The RIS node does not have the ability to transmit data in this system. In most of our simulations, we only compare the BER performance of our three proposed schemes since the conventional RIS-assisted VLC system cannot utilize RIS to send data. As such, we focus our analysis on systems where RIS can transmit data, where RIS-SM and RIS-GSM can be used as benchmarks to demonstrate the superiority of RIS-RSM. To ensure a fair comparison in our simulations, we set the bit per channel use (bpcu) to be the same, as shown in Table III. Specifically, in each transmission, LED sends a 4-PAM signal, while RIS employs spatial modulation to transmit 2 bits in the three proposed schemes. Consequently, all schemes have a bpcu equal to 4. In contrast, for the conventional RIS-assisted system, we set the modulation scheme of LED to 16-PAM, enabling it to send 4 bits in each transmission.

$$\mathrm{BER}_{\text{RIS-SM}} \le \frac{1}{MN_g \log_2(MN_g)} \sum_{g_1=1}^{N_g} \sum_{m_1=1}^{M} \sum_{g_2=1}^{N_g} \sum_{m_2=1}^{M} d_H(\mathbf{s}(g_1,m_1),\mathbf{s}(g_2,m_2)) \times Q\left(\sqrt{\frac{r^2\left\|\mathbf{s}(g_1,m_1)-\mathbf{s}(g_2,m_2)\right\|_2^2}{4\sigma^2}}\right),\ \mathbf{s}(g_j,m_j) = \mathbf{H}\mathbf{s}_{\text{RIS-SM}}(g_j)\cdot s_{\text{LED}}(m_j),\ j\in\{1,2\} \tag{16}$$

$$\mathrm{BER}_{\text{RIS-GSM}} \le \frac{1}{MN_g' \log_2(MN_g')} \sum_{g_1=1}^{N_g'} \sum_{m_1=1}^{M} \sum_{g_2=1}^{N_g'} \sum_{m_2=1}^{M} d_H(\mathbf{s}(g_1,m_1),\mathbf{s}(g_2,m_2)) \times Q\left(\sqrt{\frac{r^2\left\|\mathbf{s}(g_1,m_1)-\mathbf{s}(g_2,m_2)\right\|_2^2}{4\sigma^2}}\right),\ \mathbf{s}(g_j,m_j) = \mathbf{H}\mathbf{s}_{\text{RIS-GSM}}(g_j)\cdot s_{\text{LED}}(m_j),\ j\in\{1,2\} \tag{17}$$

$$\mathrm{BER}_{\text{RIS-RSM}} \le \frac{1}{MN_r \log_2(MN_r)} \sum_{i_1=1}^{N_r} \sum_{m_1=1}^{M} \sum_{i_2=1}^{N_r} \sum_{m_2=1}^{M} d_H(\mathbf{s}(i_1,m_1),\mathbf{s}(i_2,m_2)) \times Q\left(\sqrt{\frac{r^2\left\|(\mathbf{s}(i_1,m_1)-\mathbf{s}(i_2,m_2))\right\|_2^2}{4\sigma^2}}\right),\ \mathbf{s}(i_j,m_j) = \mathbf{h}_{\text{sum},i_j}\cdot s_{\text{LED}}(m_i),\ j\in\{1,2\} \tag{18}$$

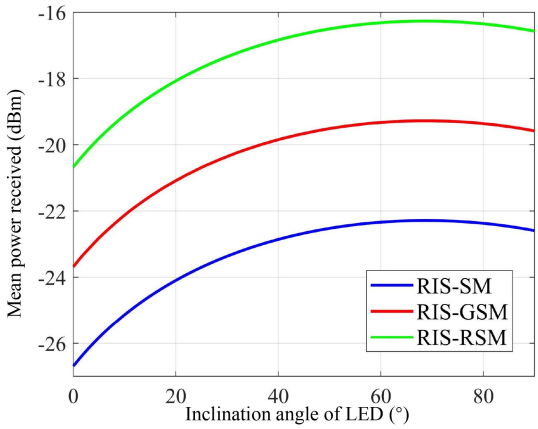

Fig. 6. Mean reception power comparison against angle of LED illumination angles. The center of PD array is placed at L1 location.

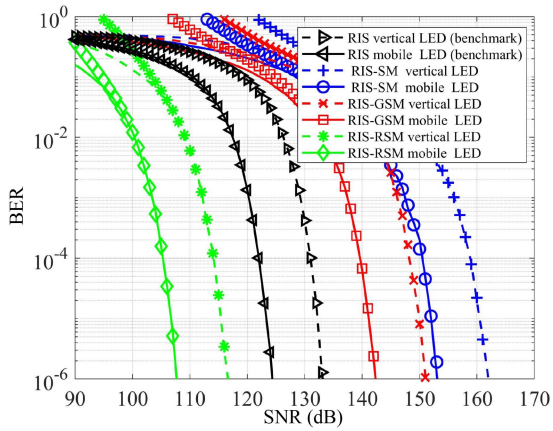

Fig. 7. BER performances of RIS-SM, RIS-GSM and RIS-RSM with vertical and mobile direction LED, where the center of PD array is located at L1.

A. Performance Analysis With Unblocked NLOS Links and Blocked LOS Links

We first analyze the influence of the transmitter direction. In Fig. 6, we show how the average received power changes with the pointing direction of LED, where inclination angle is 0° means the LED is vertical, and the mean power received of the three schemes can be evaluated by utilizing the derived average channel gain values in (6), (8) and (10), respectively. As can be seen, the average received power will first become higher and then decrease as the inclination angle increases. The separation point is about 68.2°, which is exactly the direction pointing to the center of RIS. This means that a mobile direction LED pointing to the center of RIS can lead to a maximum received power, because the emergence angle of LED in this case is small and results in a low channel attenuation. Under a fixed inclination angle, the average received energy depend on the number of channels and the corresponding channel gains. As the light power generated by LED is constant, and RIS only controls the number of active channels, rather than changing the amplitude of incident light, the received energy is influenced by the number of active RIS groups. As a result, we can see from Fig. 6 that RIS-SM exhibits the lowest received power, while RIS-RSM demonstrates the highest value. This discrepancy arises because RIS-SM activates only one RIS group, leading to a minimum reflected power, whereas RIS-RSM keeps all groups active, resulting in a maximum reflected power.

In Fig. 7, we show the BER performance of the proposed RIS enabled spatial modulation schemes, where the red, blue and green lines are simulation results of RIS-SM, RIS-GSM and RIS-RSM, respectively, and the markers are the corresponding numerical upper bounds derived from (16), (17) and (18). Here "SNR" is defined as the ratio of *transmitted* signal energy to noise. The term "vertical LED" means the LED is vertical, while "mobile LED" means that the direction of LED is set to point to the center of RIS. As can be seen, the derived upper bound is tight, especially at high SNRs, which shows the validity of our analysis in Section III-C. We can also see that the use of mobile LED can effectively enhance the BER performance compared with the vertical direction LED configuration, which is the same as the conclusion in Fig. 6. In the following simulations, we will set the LED as a "mobile LED", i.e., its direction is pointed to the center of RIS.

In Fig. 7, we also show the BER performance of the conventional RIS-assisted system for comparison, and they are named as "RIS vertical LED" and "RIS mobile LED", as shown by the black lines in Fig. 7. As can be seen, under the same bpcu, the conventional system outperforms RIS-SM and RIS-GSM. This is because the conventional system only transmits the PAM signal generated by LED and does not transmit data in the spatial domain, eliminating the channel correlation problem present in RIS-SM and RIS-GSM. Besides, all RIS elements can be employed for reflecting the light signal, resulting in a higher received power. Furthermore, we can see that the conventional system has a worse BER performance than RIS-RSM. This is because in RIS-RSM, the RIS elements can also be fully exploited. Although RIS-RSM transmits data in the spatial domain, it does not suffer from high channel correlation like RIS-SM and RIS-GSM. Additionally, the PAM signal constellations generated by LED in RIS-RSM have a larger minimum Euclidean distance compared to the conventional system (since the parameter M used in RIS-RSM is smaller than that in the conventional system). As a result, RIS-RSM outperforms the other designs and achieves the best performance.

Then we show the influence of number of RIS elements N_e. Here the size of RIS is fixed, thus the increasing of N_e means that the elements will be denser and the received signal intensity will be enhanced. In Fig. 8, we can see that the BER of all the systems decrease with an increasing of the number of RIS elements. As a result, to improve the BER performance of the system, adding the number of RIS elements and changing the LED pointing direction are both effective methods.

Next we compare the performance of the system with different bpcu. As the signal contains data from LED and RIS, changing M and N_g can both alter bpcu. In Fig. 9, we show the results with different M for M-PAM used in LED. When M is larger, the BER performance becomes worse, because the minimum Euclidean distance between the signal constellations becomes smaller. Changing M in the systems will not affect the channel

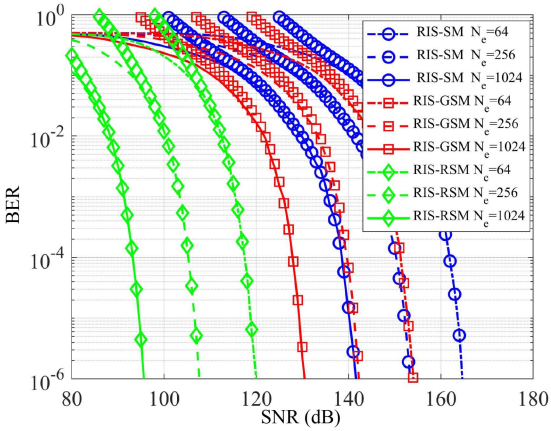

Fig. 8. BER performances of RIS-SM, RIS-GSM and RIS-RSM with different RIS elements, where the center of PD array is located at L1, $N_e = 64$, 256, and 1024.

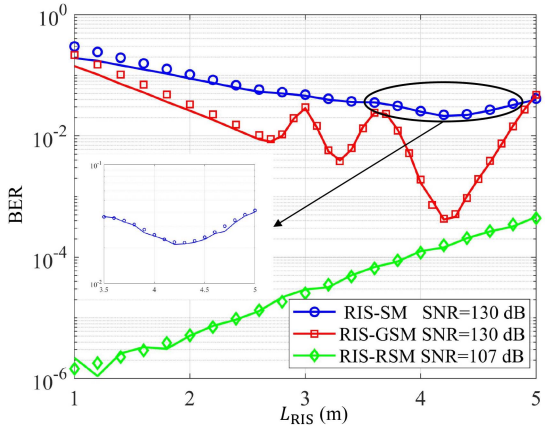

Fig. 10. BER performances of RIS-SM, RIS-GSM and RIS-RSM with different RIS size L_{RIS}, where the center of PD array is located at L1.

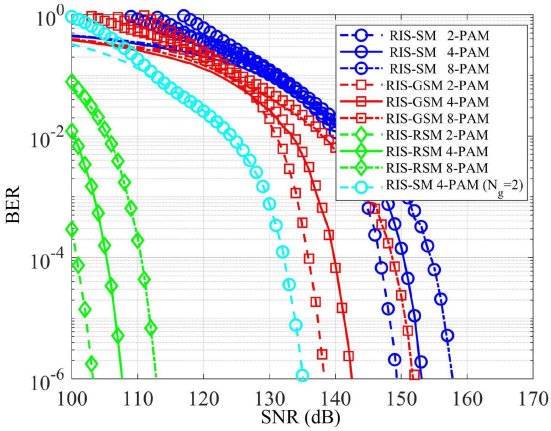

Fig. 9. BER performances of RIS-SM, RIS-GSM and RIS-RSM with different bpcu, where the center of PD array is located at L1, $M = 2$, 4, or 8 with $N_g = 4$, or $N_g = 2$ with $M = 4$.

conditions. However, the alternative of N_g can introduce a large difference to the channels. On the one hand, as we set the total number of RIS elements fixed, smaller (or bigger) N_g means more (or less) RIS elements in one group, which contributes to a more (or less) receive energy at the PD array. On the other hand, N_g is smaller (or bigger) means less (or more) channels will be available and the channel correlation will be less (or more) severe. In Fig. 9, we also show the results with $N_g = 2$. As can be seen, changing N_g has a more remarkable influence compared with M.

When the space of RIS elements becomes larger, spatial correlation will be lower. In Fig. 10, we show the BER performance against RIS elements' spaces (i.e., the length of RIS), where the link distance between RIS and PD is kept constant. Based on the simulation results, we have the following observations:

- With the increasing of L_{RIS}, BER of RIS-SM will first decrease and then increase, and there exists an optimal value of L_{RIS}. On the one hand, the channel correlation gets weaker because the coefficients between each channel become dissimilar as L_{RIS} increases (note that we divide the RIS group along the side with length L_{RIS}), which can potentially lead to an improved performance. However, on the other hand, the signal power received by the PD array will be reduced, i.e., a higher attenuation occurs with the increasing of L_{RIS}. Taking these factors into consideration, there exists a trade-off between the channel correlation coefficients and the received signal power. Consequently, an optimal value of L_{RIS} can be observed for RIS-SM in Fig. 10, balancing the benefits of reduced channel correlation with the need for sufficient signal power.
- With respect to the RIS-GSM curve, we can see that its variation in BER differs from that in RIS-SM. This is because multiple channels are combined together in RIS-GSM. As a result, the correlation coefficients do not exhibit a monotonic variation with L_{RIS}. This non-monotonic behavior can impact the BER performance in a different manner compared with RIS-SM, leading to distinct results.
- As for RIS-RSM, we observe that its BER monotonically increases with L_{RIS}. This behavior can be attributed to the fact that RIS-RSM does not suffer from the channel correlation issue, and the received energy is reduced as L_{RIS} increases, leading to a degradation in BER performance.

The signal received by the PD array contains two kinds of data: from LED and RIS. In Fig. 11, we analyze the BER of data from different sources, where $M = 4$ and $N_g = 4$, i.e., the LED and RIS have the same data rate. As can be seen, the error rate from RIS is higher for RIS-SM and RIS-GSM, while it is lower for RIS-RSM. This is because in the former two schemes, a severe channel correlation occurs and the signal in the spatial domain is the bottleneck of the system, thus their data from RIS have more errors. On the contrary, RIS-GSM has a higher error rate for LED data, because its signal in spatial domain can be recognized easily, thus the bottleneck is from the LED side.

In Fig. 11, we have shown that the BER of RIS is higher in the high channel correlation conditions. We further analyze how channel correlation affects the data error rate from both sources in RIS-SM, as shown in Fig. 12, where we set $M = N_g = 2$, (i.e., bpcu $= 2$). As can be seen, the difference between BER

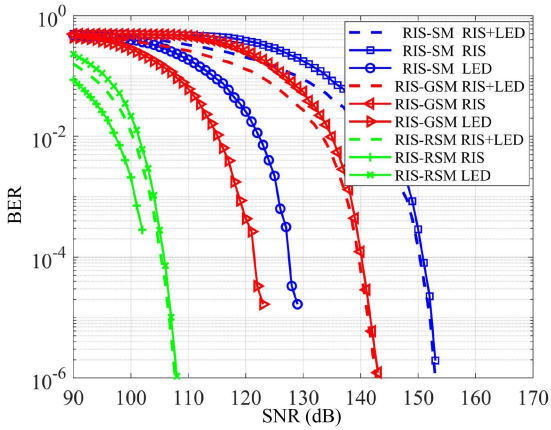

Fig. 11. BER of data from LED and RIS in RIS-SM, RIS-GSM and RIS-RSM, where the center of PD array is located at L1.

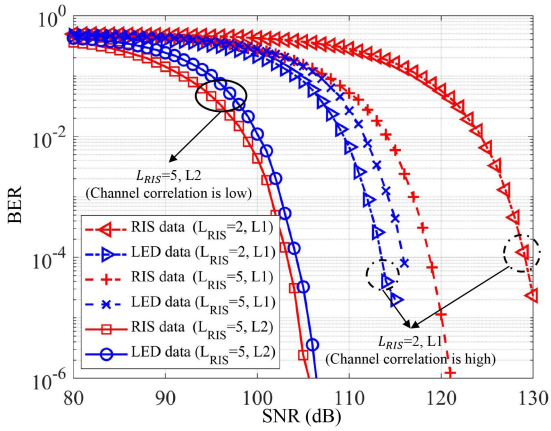

Fig. 12. BER of data from LED and RIS in RIS-SM, where $M = 2$ and $N_g = 2$, the center of PD array is located at L1 or L2.

of RIS and LED first gets smaller when the channel correlation is lower (about 15 dB at BER of 1e-3, while this value is about 24 dB in Fig. 11 with bpcu $= 4$). We then enlarge the length of RIS by setting $L_{RIS} = 5$ m, and the difference between the two error rates becomes smaller. Furthermore, when the location of the PD array is set to L2, where the two channel coefficients are more different, we can see that the data from LED has a larger BER, meaning that it is the bottleneck. As a result, when the channel correlation problem is severe, the whole system performance is limited by the signal in spatial domain and the data from RIS has more errors; while in less correlated channels, BER of LED signal is higher and becomes the bottleneck of the whole system.

B. Performance Analysis With Partially Blocked NLOS and LOS Links

In this subsection, we evaluate the system BER performance in the presence of blockages. We first consider the case that there exist different levels of blockages in NLOS links, and the the LOS links are still totally blocked. Fig. 13 depicts the BER performances of the three proposed schemes under different levels of link blockage, with $T = 0$ representing the scenarios

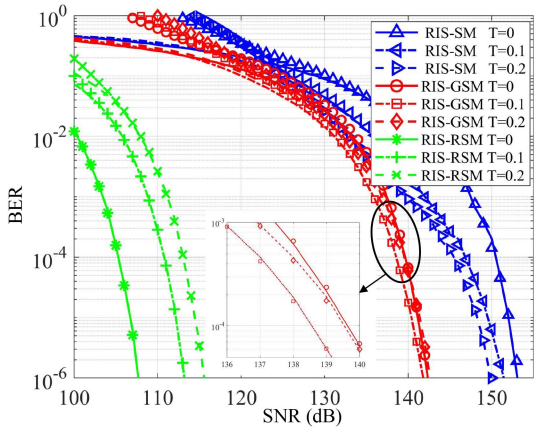

Fig. 13. BER performances of RIS-SM, RIS-GSM and RIS-RSM with different levels of blocking objects in NLOS links (LOS links are totally blocked), where the center of PD array is located at L1.

where the links cannot be blocked and serve as the benchmarks for comparison. The observations from the figure are as follows:

- For RIS-SM, inducing link blockage can lead to an improved performance, with a lower BER achieved as the level of blockage increases. This is because RIS-SM suffers from the high channel correlation problem. When some of the links are blocked, the coefficients between each channel will become less similar, resulting in reduced channel correlation. RIS-SM benefits from this reduced correlation, despite the potential decrease in received signal power.
- On the other hand, for RIS-GSM and RIS-RSM, which are less affected by channel correlation, the introduction of link blockage does not provide the same level of gain as in RIS-SM. In RIS-GSM, the gain is not obvious, and when the level of blockage increases, the BER will increase due to the reduced signal power playing a more prominent role.
- In RIS-RSM, where there is no channel correlation issue, the presence of link blockage primarily results in a lower received power which degrades the BER performance.

From Figs. 6–13, we only use NLOS links for transmission and LOS links are always blocked. Now we consider the system where LOS can also be employed for communication and evaluate the system performance in presence of blockages for all links. In this system, LOS links do not contain data from RIS because spatial modulation is performed on the RIS node that is irrelevant to LOS links. Although the induced of LOS links can enhance received power, it may also introduce interference to the NLOS signals that contain data from RIS.

In Fig. 14, we present the BER performances where both LOS and NLOS links can be blocked with some probabilities, and the conventional RIS-assisted system is used as a benchmark (named as "benchmark RIS"). Furthermore, the system with only LOS links is also plotted for comparison (named as "benchmark no RIS"). We can get the following observations:

- In RIS-SM, the performance can still be better when a higher level of blockage exists in both LOS and NLOS links. This is because the channel coefficients become less similar and channel correlation is lower.

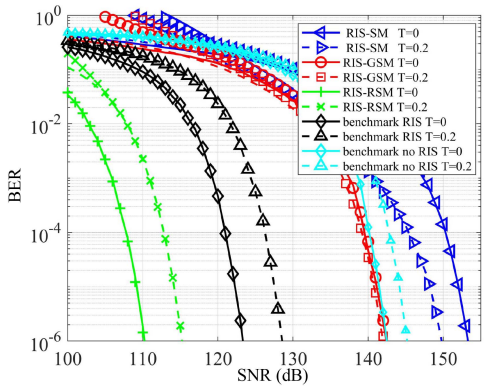

Fig. 14. BER performances of RIS-SM, RIS-GSM and RIS-RSM with different levels of blocking objects in both LOS and NLOS links, where the center of PD array is located at L1.

- For RIS-GSM, the benefits of blocking channels are relatively limited compared to those shown in Fig. 13. This is because when LOS links are considered, the PD array can receive more energy in each transmission process, and the presence of blockage leads to an increased path loss, degrading the BER performance. Furthermore, due to the comparatively lower impact of channel correlation on RIS-GSM, the gains obtained from blocking channels are relatively small.
- For RIS-RSM that does not have the channel correlation problem, the blockages will only cause a degradation of performance. Besides, when there is no blockage in the links (i.e., $T = 0$), RIS-RSM exhibits a larger BER compared to the situation without LOS links (as shown in Fig. 13). This is because the data from RIS only exists in NLOS signals, and the introduction of LOS links will be an interference, negatively impacting the performance of RIS-RSM.
- In the benchmarks where RIS cannot send its own data, we can see that blockages will degrade the BER performance, and the system with RIS demonstrates a significant improvement compared to that without RIS. This highlights the clear advantage of utilizing RIS in VLC systems.

V. Conclusions and Future Work

In this paper, we studied three RIS based spatial modulation schemes, i.e., RIS-SM, RIS-GSM and RIS-RSM, where the spatial modulation is performed by RIS to convey its own information. The theoretical upper bounds on BER are derived based on the union bound methods and Monto Carlo simulation results show the tightness of the bounds, validating the effectiveness of our analysis. According to the simulation results, we show that RIS-RSM always outperforms the other two proposed schemes for its employing RIS more effectively and lower channel correlation. Besides, adjusting the direction of LED and using more RIS elements can contribute to an improvement in BER performance due to the less path loss and more receive energy.

Another important finding is that the increasing of the total system's bpcu may cause BER degradation. For example, changing RIS group numbers is a simple way to change bpcu, and it may have a remarkable influence on BER, because the channel coefficients are changed drastically. We also analyze how channel correlation problem influence the system performance. If the channel coefficients are approximately the same, the data from RIS transmitted in the spatial domain have a higher error rate. However, if the channels are less correlated, for example, using a RIS with larger size, or RIS-RSM scheme, then the system BER is mainly limited by the data from LED. Thus there is a trade-off between the dominating source of errors considering the channel correlation coefficients. Furthermore, we evaluate the system BER performance in the presence of different levels of link blockages. For RIS-SM that is affected by high channel correlation, higher level of blockage can reduce BER. However, for RIS-RSM, blockage may cause a higher path loss, and hence degrades the BER performance.

As for future work, first, practical system implementation of RIS enabled spatial modulation schemes in VLC is challenging, as the materials enabling RIS control function is hard to obtain. Second, our current study on the link blockage is based on numerical simulations, and thorough theoretical analysis on the system performance with link blockages may lead to better understanding of RIS enabled VLC systems. Last, the current placement orientation of each PD is straight to the ceiling, random PD directions in practical system may have more complicated BER results.

References

[1] D. Karunatilaka, F. Zafar, V. Kalavally, and R. Parthiban, "LED based indoor visible light communications: State of the art," *IEEE Commun. Surveys Tut.*, vol. 17, no. 3, pp. 1649–1678, thirdquarter 2015.

[2] Z. Zhang et al., "6G wireless networks: Vision, requirements, architecture, and key technologies," *IEEE Veh. Technol. Mag.*, vol. 14, no. 3, pp. 28–41, Sep. 2019.

[3] T. Huang, W. Yang, J. Wu, J. Ma, X. Zhang, and D. Zhang, "A survey on green 6G network: Architecture and technologies," *IEEE Access*, vol. 7, pp. 175758–175768, 2019.

[4] L. E. M. Matheus, A. B. Vieira, L. F. M. Vieira, M. A. M. Vieira, and O. Gnawali, "Visible light communication: Concepts, applications and challenges," *IEEE Commun. Surveys Tut.*, vol. 21, no. 4, pp. 3204–3237, Fourthquarter 2019.

[5] R. Alghamdi et al., "Intelligent surfaces for 6G wireless networks: A survey of optimization and performance analysis techniques," *IEEE Access*, vol. 8, pp. 202795–202818, 2020.

[6] Q. Wu and R. Zhang, "Towards smart and reconfigurable environment: Intelligent reflecting surface aided wireless network," *IEEE Commun. Mag.*, vol. 58, no. 1, pp. 106–112, Jan. 2020.

[7] X. Wang and G.-M. Yang, "Time-coding spread-spectrum reconfigurable intelligent surface for secure wireless communication: Theory and experiment," *Opt. Exp.*, vol. 29, no. 20, pp. 32031–32041, Sep. 2021. [Online]. Available: https://opg.optica.org/oe/abstract.cfm?URI=oe-29-20-32031

[8] M. Munochiveyi, A. C. Pogaku, D.-T. Do, A.-T. Le, M. Voznak, and N. D. Nguyen, "Reconfigurable intelligent surface aided multi-user communications: State-of-the-art techniques and open issues," *IEEE Access*, vol. 9, pp. 118584–118605, 2021.

[9] H. Abumarshoud, L. Mohjazi, O. A. Dobre, M. Di Renzo, M. A. Imran, and H. Haas, "LiFi through reconfigurable intelligent surfaces: A new frontier for 6G?," *IEEE Veh. Technol. Mag.*, vol. 17, no. 1, pp. 37–46, Mar. 2022.

[10] S. Sun, T. Wang, F. Yang, J. Song, and Z. Han, "Intelligent reflecting surface-aided visible light communications: Potentials and challenges," *IEEE Veh. Technol. Mag.*, vol. 17, no. 1, pp. 47–56, Mar. 2022.

[11] A. M. Abdelhady, O. Amin, M.-S. Alouini, and B. Shihada, "Revolutionizing optical wireless communications via smart optics," *IEEE Open J. Commun. Soc.*, vol. 3, pp. 654–669, 2022.

[12] H. Ajam, M. Najafi, V. Jamali, B. Schmauss, and R. Schober, "Modeling and design of IRS-assisted multilink FSO systems," *IEEE Trans. Commun.*, vol. 70, no. 5, pp. 3333–3349, May 2022.

[13] M. Najafi, B. Schmauss, and R. Schober, "Intelligent reflecting surfaces for free space optical communication systems," *IEEE Trans. Commun.*, vol. 69, no. 9, pp. 6134–6151, Sep. 2021.

[14] S. Aboagye, T. M. N. Ngatched, O. A. Dobre, and A. R. Ndjiongue, "Intelligent reflecting surface-aided indoor visible light communication systems," *IEEE Commun. Lett.*, vol. 25, no. 12, pp. 3913–3917, Dec. 2021.

[15] A. R. Ndjiongue, T. M. N. Ngatched, O. A. Dobre, and H. Haas, "Toward the use of re-configurable intelligent surfaces in VLC systems: Beam steering," *IEEE Wireless Commun.*, vol. 28, no. 3, pp. 156–162, Jun. 2021.

[16] H. Abumarshoud, B. Selim, M. Tatipamula, and H. Haas, "Intelligent reflecting surfaces for enhanced NOMA-based visible light communications," in *Proc. IEEE Int. Conf. Commun.*, 2022, pp. 571–576.

[17] Y. Yang et al., "Low complexity OFDM VLC system enabled by spatial summing modulation," *Opt. Exp.*, vol. 27, no. 21, pp. 30788–30795, Oct. 2019. [Online]. Available: https://opg.optica.org/oe/abstract.cfm?URI=oe-27-21-30788

[18] P. H. Pathak, X. Feng, P. Hu, and P. Mohapatra, "Visible light communication, networking, and sensing: A survey, potential and challenges," *IEEE Commun. Surveys Tut.*, vol. 17, no. 4, pp. 2047–2077, Fourthquarter 2015.

[19] H. Marshoud, P. C. Sofotasios, S. Muhaidat, and G. K. Karagiannidis, "Multi-user techniques in visible light communications: A survey," in *Proc. Int. Conf. Adv. Commun. Syst. Inf. Secur.*, 2016, pp. 1–6.

[20] H. Q. Ngo, E. G. Larsson, and T. L. Marzetta, "Energy and spectral efficiency of very large multiuser MIMO systems," *IEEE Trans. Commun.*, vol. 61, no. 4, pp. 1436–1449, Apr. 2013.

[21] R. Y. Mesleh, H. Haas, S. Sinanovic, C. W. Ahn, and S. Yun, "Spatial modulation," *IEEE Trans. Veh. Technol.*, vol. 57, no. 4, pp. 2228–2241, Jul. 2008.

[22] L. Deng and Y. Fan, "Analysis of channel correlation and channel capacity for indoor MIMO visible light communication systems," *Appl. Opt.*, vol. 59, no. 15, pp. 4672–4684, May 2020. [Online]. Available: https://opg.optica.org/ao/abstract.cfm?URI=ao-59-15-4672

[23] R. Bai, R. Jang, J. Tan, and J. Quan, "Performance comparison of VLC MIMO techniques considering indoor illuminance with inclined LEDs," in *Proc. IEEE Int. Conf. Wireless Space Extreme Environ.*, 2016, pp. 105–110.

[24] T. Fath and H. Haas, "Performance comparison of MIMO techniques for optical wireless communications in indoor environments," *IEEE Trans. Commun.*, vol. 61, no. 2, pp. 733–742, Feb. 2013.

[25] F. Shu et al., "Spatial modulation: An attractive secure solution to future wireless networks," *IEEE Netw.*, vol. 36, no. 3, pp. 130–135, May/Jun. 2022.

[26] M. Wen et al., "A survey on spatial modulation in emerging wireless systems: Research progresses and applications," *IEEE J. Sel. Areas Commun.*, vol. 37, no. 9, pp. 1949–1972, Sep. 2019.

[27] C. Zhong, X. Hu, X. Chen, D. W. K. Ng, and Z. Zhang, "Spatial modulation assisted multi-antenna non-orthogonal multiple access," *IEEE Wireless Commun.*, vol. 25, no. 2, pp. 61–67, Apr. 2018.

[28] A. B. Saleem, S. A. Hassan, H. Jung, S. Garg, G. Kaddoum, and M. Guizani, "Full-duplex quadrature spatial modulation for multi-antenna systems," *IEEE Netw.*, vol. 35, no. 5, pp. 226–233, Sep./Oct. 2021.

[29] Q. Li, M. Wen, and M. Di Renzo, "Single-RF MIMO: From spatial modulation to metasurface-based modulation," *IEEE Wireless Commun.*, vol. 28, no. 4, pp. 88–95, Aug. 2021.

[30] R. Mesleh, H. Elgala, and H. Haas, "Optical spatial modulation," *J. Opt. Commun. Netw.*, vol. 3, no. 3, pp. 234–244, 2011.

[31] S. P. Alaka, T. L. Narasimhan, and A. Chockalingam, "Generalized spatial modulation in indoor wireless visible light communication," in *Proc. IEEE Glob. Commun. Conf.*, 2015, pp. 1–7.

[32] A. Stavridis and H. Haas, "Performance evaluation of space modulation techniques in VLC systems," in *Proc. IEEE Int. Conf. Commun. Workshop*, 2015, pp. 1356–1361.

[33] D. Li, W. Zhang, J. Sun, and C.-X. Wang, "An improved generalized spatial modulation scheme for indoor visible light communications," in *Proc. IEEE/CIC Int. Conf. Commun. China*, 2017, pp. 1–5.

[34] X. Gao, Z. Bai, P. Gong, and D. O. Wu, "Design and performance analysis of LED-grouping based spatial modulation in the visible light communication system," *IEEE Trans. Veh. Technol.*, vol. 69, no. 7, pp. 7317–7324, Jul. 2020.

[35] F. Wang, F. Yang, and J. Song, "Constellation optimization under the ergodic VLC channel based on generalized spatial modulation," *Opt. Exp.*, vol. 28, no. 14, pp. 21202–21209, Jul. 2020. [Online]. Available: https://opg.optica.org/oe/abstract.cfm?URI=oe-28-14-21202

[36] S. Naser, L. Bariah, S. Muhaidat, M. Al-Qutayri, M. Uysal, and P. C. Sofotasios, "Space-time block coded spatial modulation for indoor visible light communications," *IEEE Photon. J.*, vol. 14, no. 1, Feb. 2022, Art. no. 7303111.

[37] E. Basar, "Reconfigurable intelligent surface-based index modulation: A new beyond MIMO paradigm for 6G," *IEEE Trans. Commun.*, vol. 68, no. 5, pp. 3187–3196, May 2020.

[38] W. Yan, X. Yuan, and X. Kuai, "Passive beamforming and information transfer via large intelligent surface," *IEEE Wireless Commun. Lett.*, vol. 9, no. 4, pp. 533–537, Apr. 2020.

[39] S. Lin, B. Zheng, G. C. Alexandropoulos, M. Wen, M. D. Renzo, and F. Chen, "Reconfigurable intelligent surfaces with reflection pattern modulation: Beamforming design and performance analysis," *IEEE Trans. Wireless Commun.*, vol. 20, no. 2, pp. 741–754, Feb. 2021.

[40] T. Ma, Y. Xiao, X. Lei, P. Yang, X. Lei, and O. A. Dobre, "Large intelligent surface assisted wireless communications with spatial modulation and antenna selection," *IEEE J. Sel. Areas Commun.*, vol. 38, no. 11, pp. 2562–2574, Nov. 2020.

[41] S. Guo, J. Ye, P. Zhang, H. Zhang, and M.-S. Alouini, "Differential reflecting modulation for reconfigurable intelligent surface-based communications," *IEEE Commun. Lett.*, vol. 25, no. 3, pp. 907–910, Mar. 2021.

[42] L. Zhang, X. Lei, Y. Xiao, and T. Ma, "Large intelligent surface-based generalized index modulation," *IEEE Commun. Lett.*, vol. 25, no. 12, pp. 3965–3969, Dec. 2021.

[43] S. Lin, M. Wen, M. Di Renzo, and F. Chen, "Reconfigurable intelligent surface-based quadrature reflection modulation," in *Proc. IEEE Int. Conf. Commun.*, 2021, pp. 1–6.

[44] M. D. Renzo et al., "Smart radio environments empowered by reconfigurable AI meta-surfaces: An idea whose time has come," *EURASIP J. Wireless Commun. Netw.*, vol. 2019, no. 1, pp. 1–20, 2019.

[45] S. Lin, F. Chen, M. Wen, Y. Feng, and M. D. Renzo, "Reconfigurable intelligent surface-aided quadrature reflection modulation for simultaneous passive beamforming and information transfer," *IEEE Trans. Wireless Commun.*, vol. 21, no. 3, pp. 1469–1481, Mar. 2022.

[46] E. Panayirci, M. Koca, H. Haas, and H. V. Poor, "Spatial modulation aided physical layer security for NOMA-VLC systems," *IEEE Trans. Veh. Technol.*, early access, Mar. 24, 2023, doi: 10.1109/TVT.2023.3257362.

[47] Z. Ghassemlooy, W. Popoola, and S. Rajbhandari, *Optical Wireless Communications: System and Channel Modelling With Matlab*. Boca Raton, FL, USA: CRC, 2019.

[48] S. Sun, F. Yang, J. Song, and R. Zhang, "Intelligent reflecting surface for MIMO VLC: Joint design of surface configuration and transceiver signal processing," *IEEE Trans. Wireless Commun.*, early access, Jan. 20, 2023, doi: 10.1109/TWC.2023.3236811.

[49] A. M. Abdelhady, A. K. S. Salem, O. Amin, B. Shihada, and M.-S. Alouini, "Visible light communications via intelligent reflecting surfaces: Metasurfaces vs mirror arrays," *IEEE Open J. Commun. Soc.*, vol. 2, pp. 1–20, 2021.

[50] J. Jeyadeepan, G. Ali, and S. Leszek, "Spatial modulation: Optimal detection and performance analysis," *IEEE Commun. Lett.*, vol. 12, no. 8, pp. 545–547, Aug. 2008.

[51] Y. Abdelhamid, S. Sinan, D. R. Marco, M. Raed, and H. Harald, "Generalised sphere decoding for spatial modulation," *IEEE Trans. Commun.*, vol. 61, no. 7, pp. 2805–2815, Jul. 2013.

[52] J. Proakis and M. Salehi, *Digital Communications*. New York, NY, USA: McGraw-Hill, 2008. [Online]. Available: https://books.google.com.hk/books?id=ABSmAQAACAAJ

[53] N. R. Prasad and C. Wan-Young, "Evaluation of reconfigurable intelligent surface-assisted underwater wireless optical communication system," *J. Lightw. Technol.*, vol. 40, no. 13, pp. 4257–4267, Jul. 2022.

[54] H. Wang et al., "Performance of wireless optical communication with reconfigurable intelligent surfaces and random obstacles," 2020, *arXiv:2001.05715*.